# Surface structure and lattice dynamics of KI(001) studied by high-resolution ion scattering combined with molecular dynamics simulation

T. Okazawa, T. Nishimura, and Y. Kido*
*Department of Physics, Ritsumeikan University, Kusatsu, Shiga-ken 525-8577, Japan*
(Received 19 April 2002; published 4 September 2002)

The rumpled surface structure and thermal lattice vibrations of KI(001) were studied by high-resolution medium-energy ion scattering (MEIS) and molecular dynamics (MD) simulation. The relaxation of the interlayer distance between the top and second layer and the rumpling of the top and second layers were measured directly by MEIS with an accuracy of 0.01 Å. From the displaced lattice positions determined above, we derived the dipole moments of the top- and second-layer $K^+$ and $I^-$ ions self-consistently using the polalizabilities estimated from the optical refractive index combined with the Clausius-Mossotti relation. The balance between a short-range force and a long-range Coulombic one made it possible to judge the applicability of the short-range pair potentials proposed so far. We also determined the root-mean-square thermal vibration amplitudes of the bulk and top-layer ions together with the correlations between the top- and second-layer ions by means of the ion shadowing effect applied to various kinds of scattering geometries. The results obtained were compared with those calculated from the MD simulations based on a semiclassical model using the dipole moments determined above and a Born-Mayer- or Hellmann-type pair potential. The present results are in overall agreement with the MD simulations employing the pair potential proposed by Catlow *et al.* [J. Phys. C **10**, 1395 (1977)].

DOI: 10.1103/PhysRevB.66.125402 PACS number(s): 68.35.Ja, 61.85.+p, 78.55.Fv

## I. INTRODUCTION

It is well known that alkali-halide crystals have strongly relaxed and rumpled surfaces, because the electric fields at the lattice sites of the near-surface region are not completely canceled out and as a result the ions near the surface have dipole moments.[1] Such a characteristic surface structure would generate a specific nature of the lattice motion. For example, a crystal row consisting of alternating plus and minus point charges would induce strongly correlated thermal vibrations because of the attractive force between the neighboring ions. Unfortunately, there are only a few reports not only on the structural analysis, but also on the lattice dynamics of the alkali-halide surfaces.[2–4] The reason is probably due to the large band gaps leading to intense charge-up by x-ray, electron, and ion irradiations. Concerning the theoretical investigations, semiclassical shell models[5–8] have been developed and they predicted the structures and dispersion relations for the surfaces. For more precise analysis of the surface structure, it needs a fully quantum mechanical approach. Recently, a challenge has been done to determine the optimized surface structure of alkali-halide crystals using an *ab initio* molecular dynamics (MD) calculation based on density functional theory.[9]

In this study, we first determine the rumpled surface structure of KI(001) by high-resolution medium-energy ion scattering (MEIS). Then the dipole moments of the top- and second-layer $K^+$ and $I^-$ ions are derived self-consistently from the above displaced lattice positions. Here we use the polarizabilities of both ions estimated from the observed refraction data coupled with the Clausisu-Mossotti relation. If one regards the lattice site ion as a point charge accompanied by a dipole moment, the balance between a Born-Mayer- or Hellmann-type short-range force and a long-range Coulombic one can judge the applicability of the short-range pair potentials proposed so far. We also determine the root-mean-square (rms) thermal vibration amplitudes (TVA's) of the bulk and top-layer ions together with the correlations between the top- and second-layer ions. In order to derive the above values directly by means of MEIS, the ion shadowing and focusing effects are applied to various kinds of scattering geometries. The results are compared with the predictions given by the semiclassical MD simulations employing the dipole moments determined here and the applicable pair potential.

## II. EXPERIMENT

The KI(001) crystals (lattice constant 7.066 Å) with purity better than 99.99% were purchased from the Optoelectronic Materials Laboratory of the University of Utah. We prepared the clean KI(001) surface by cleaving the rod with a razor blade in $N_2$ ambience and then immediately introduced it into an ultrahigh-vacuum (UHV) chamber. The sample was mounted on a six-axis goniometer and heated to 100–150 °C for 5 min in UHV ($2\times10^{-10}$ Torr). The clean surface without carbon and oxygen contamination was confirmed, respectively, by Auger electron and ultraviolet photoelectron spectroscopy.

We used 70-keV $He^+$ beams which were collimated to 0.05 (horizontal) $\times$2.0 (vertical) $mm^2$. The backscattered $He^+$ ions were detected by a high-resolution toroidal electrostatic analyzer (ESA) mounted on a turntable. It has a wide interelectrode distance of 16 mm and thus covers a broad energy range (10% of the pass energy) at a fixed applied voltage.[10] After the electric deflection, the ions impinge on a three-stage microchannel plates combined with a silicon position-sensitive detector (PSD), which has an excellent position resolution of 40 $\mu$m. Our toroidal ESA makes it pos-

 

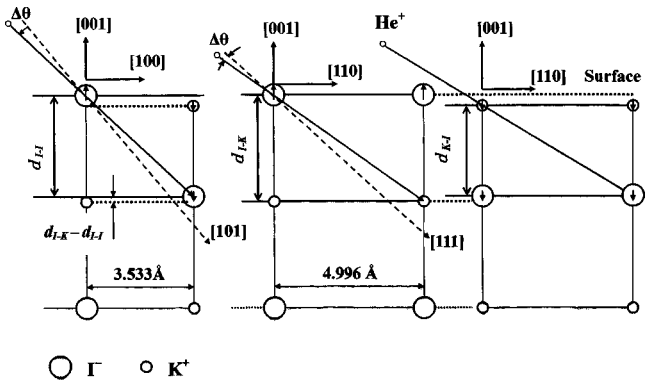


FIG. 1. Side views of three kinds of $He^+$ incidence on KI(001) surfaces. (i) Left: He ions are incident along the [101] axis and the scattering plane is (010). (ii) Center: incidence along the $I^-$-terminated [111] axis in the $(1\bar{1}0)$ plane. (iii) Right: incidence along the $K^+$-terminated [111] axis in the $(1\bar{1}0)$ plane.

sible to clearly see a blocking pattern on the PSD image, and thus it is easy to set up a desired scattering condition for outgoing ions such as blocking-focusing and random geometries. The angular resolution was estimated to be better than 0.1° from reproducibility of angular yield curves. In order to suppress a charge-up effect, the sample surface was covered with thin Al foils except for a small ion-irradiation area. The beam position on the sample surface was shifted by 1 mm in the horizontal plane after an integration beam current of 1 $\mu$C to avoid the accumulation of radiation damages.

### III. STRUCTURE ANALYSIS

First, we determine the heights ($d_{\text{I-I}}, d_{\text{K-I}}$) of the top-layer $I^-$ and $K^+$ ions from the second-layer $I^-$ ions. In this case, two energy windows were set for the scattering components from the second-layer $I^-$ ions and from the deeper layers $I^-$ ions. Then angular scans were performed for the above two scattering components around the [101] axis in the (010) plane and around the [111] axis in the $(1\bar{1}0)$ plane. The former angular scan gives the height of the top-layer $I^-$ ions and the latter that of the top-layer $K^+$ ions scaled from the second-layer $I^-$ ions. We also set an energy window for the scattering component from the second-layer $K^+$ ions and performed the angular scan around the [111] axis and in the $(1\bar{1}0)$ plane. It gives the height ($d_{\text{I-K}}$) of the top-layer $I^-$ ions scaled from the second-layer $K^+$ ions. The situation is illustrated in Fig. 1 and the details of such a procedure are referred to the literature.[2,3]

Figure 2 shows a typical MEIS spectrum observed for 70-keV $He^+$ ions incident along the [101] axis and backscattered to 80° (random direction) from $I^-$ ions in the (010) plane. The spectrum was decomposed into the scattering component (Gaussian) from each layer of $I^-$ ions. The energy window for the scattering component from the second-layer $I^-$ ions was set between 66.4 and 66.7 keV. It partly includes the scattering components from the top- and third-layer $I^-$ ions. However, this does not affect the determination of the angle giving the scattering yield minimum for the

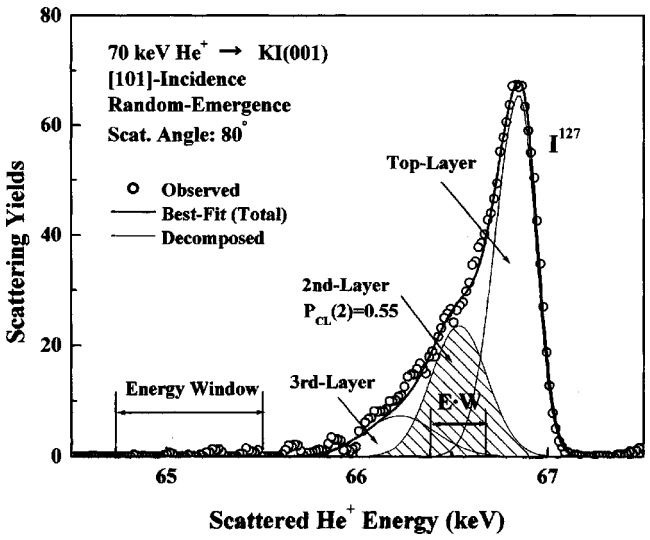


FIG. 2. Observed MEIS spectrum (open circles) for 70-keV $He^+$ ions incident along the [101] axis and backscattered to 80°. Thin and thick solids curves are the deconvoluted and total MEIS spectra, respectively, best fitted to the observed one. The scattering component from the second-layer $I^-$ ions is indicated by the shaded Gaussian shape.

scattering component from the second-layer $I^-$ ions, because of no shadowing effect for the top-layer $I^-$ ions and of a small contribution from the third-layer $I^-$ ions.

Figures 3(a) and 3(b) indicate the angular scan spectrum around the [101] axis in the (010) plane and around the [111] axis in the $(1\bar{1}0)$ plane, respectively, for the scattering component from the second-layer $I^-$ ions. The angles giving the scattering yield minima were estimated from an appropriate polynomial fitting.[3] From the angular shifts indicated in the figures, the heights of the top-layer $I^-$ and $K^+$ ions from the second-layer $I^-$ ions were determined to be $3.502 \pm 0.010$ Å ($d_{\text{I-I}}$) and $3.438 \pm 0.010$ Å ($d_{\text{K-I}}$), respectively, by the simple triangulation method.[2,3] The height of the top-layer $I^-$ ions from the second-layer $K^+$ ions was deduced to be $3.507 \pm 0.015$ Å ($d_{\text{I-K}}$). Thus the average interlayer distance between the top- and second-layer $d_{12}[=(d_{\text{I-I}}+d_{\text{I-K}}+d_{\text{K-I}}+d_{\text{K-K}})/4]$ is deduced to be 3.473 Å, namely, shrinks by 0.06 Å.

The surface relaxation ($\varepsilon$) and the rumpling of the top-layer ($\Delta\varepsilon_1$) and second-layer ($\Delta\varepsilon_2$) are defined by

$$\varepsilon = \{(d_{12} - d_{\text{bulk}})/d_{\text{bulk}}\} \times 100 \ (\%),$$

$$\Delta\varepsilon_1 = \{(d_{\text{I-I}} - d_{\text{K-I}})/d_{\text{bulk}}\} \times 100 \ (\%),$$

$$\Delta\varepsilon_2 = \{(d_{\text{I-I}} - d_{\text{I-K}})/d_{\text{bulk}}\} \times 100 \ (\%), \qquad (1)$$

where $d_{\text{bulk}}$ is the bulk interlayer distance (3.533 Å). The surface relaxation and rumpling for KI(001) at room temperature (RT) are listed in Table I and compared with the shell model calculations.[5–7] The minus sign in the relaxation means a contraction of the interlayer distance compared with the bulk interlayer distance ($d_{\text{bulk}}$), and the plus sign in the rumpling indicates a displacement of negative ions toward

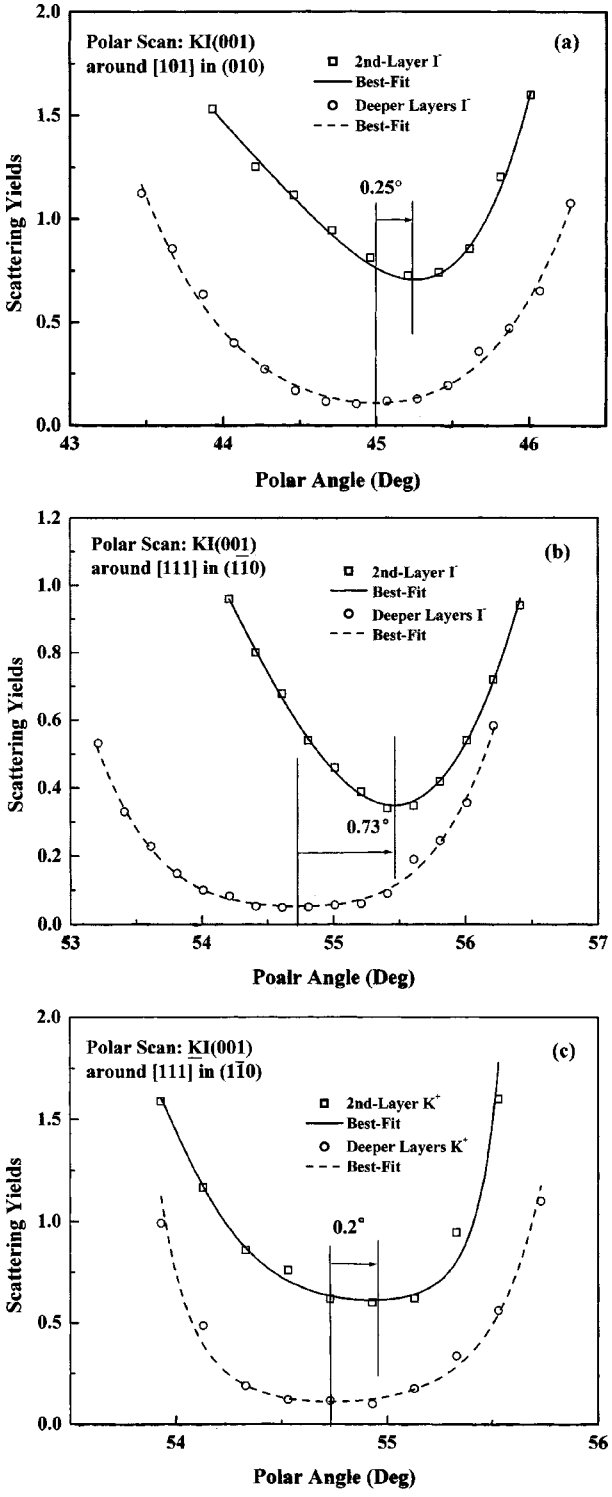


FIG. 3. Angular scan spectra for 70-keV $He^+$ ions incident around the [101] axis in the (010) plane (a) and around the [111] axis in the $(1\bar{1}0)$ plane (b) and (c). Open squares and circles denote the scattering components from the second-layer $I^-$ ions and from deeper layers ions, respectively. In the case of (c), open squares denote the scattering component from the second-layer $K^+$ ions. The scattering angle was fixed at 80° and 68° for polar scans around the [101] and [111] axis, respectively. The straight lines indicate the angles giving the scattering yield minima determined by a fourth-order polynomial curve fitting.

TABLE I. Surface relaxation ($\varepsilon$) and rumpling of top ($\Delta\varepsilon_1$) and second ($\Delta\varepsilon_2$) layer of KI (001) determined by MEIS and shell models (Refs. 5–7). In the MD* simulation, the pair potential and dipole moments given by the shell model (Ref. 5) were used.

| | $\varepsilon$ (%) | $\Delta\varepsilon_1$ (%) | $\Delta\varepsilon_2$ (%) |
|---|---|---|---|
| Present MEIS | $-1.63\pm0.4$ | $+1.78\pm0.3$ | $+0.59\pm0.4$ |
| Shell model[a] | $-1.67$ | $+5.50$ | $-3.01$ |
| Shell model[b] | $-0.80$ | $+3.99$ | |
| Shell model[c] | $-0.46$ | $+0.92$ | $-0.56$ |
| MD* | $-3.21$ | $+6.11$ | $-2.46$ |

[a]Reference 5.
[b]Reference 6.
[c]Reference 7.

the vacuum side relative to that of positive ions in the same atomic plane. Significant discrepancies are seen between the present MEIS result and the predictions by the shell models.[5–7] It suggests inaccuracies of these semiclassical shell model calculations. In the above shell model, Benson and Claxton[5] introduced a distortion energy for each layer which is expressed as a function of the displacements and dipole moments of the ions in this layer. The equilibrium configuration was determined by equating to zero the first derivatives of the distortion energy for each layer independently. Such a too simplified treatment possibly led to the inaccurate result. In fact, the MD simulation using the same interatomic potential and dipole moments does not coincide with the shell model calculation.[5]

The displacements of the top- and second-layer ions from the unrelaxed lattice positions can give their dipole moments self-consistently if the polarizability of each ion is known. The dipole moment of an ion $i$ in the $n$th layer is given by

$$\vec{\mu}_n^i = \alpha^i \sum_j \{\vec{E}_p(\vec{r}_{ij}) + \vec{E}_d(\vec{r}_{ij})\}, \tag{2}$$

where $\alpha^i$ is the polarizability of ion $i$ and $\vec{E}_p(\vec{r}_{ij})$ and $\vec{E}_d(\vec{r}_{ij})$ are, respectively, the electric fields induced by a point charge $e_j$ and by a dipole moment $\vec{\mu}_m^j$ of a lattice site ion $j$. Here $\vec{r}_{ij}$ is the position vector of the $j$th ion relative to the $i$th. We must note that the dipole moments and electric fields are directed to the surface normal direction because of the symmetric configuration in the lateral plane.[12] Both electric fields are calculated by the modified Ewald method.[13] First, we calculated the electric field induced at the ion $i$ in the top layer assuming appropriate dipole moments of the top-layer $I^-$ ($\vec{\mu}_1^-$) and $K^+$ ($\vec{\mu}_1^+$) ions. As a first approximation, the dipole moments of the underlying ions were neglected, because the deeper the lattice site positions, the smaller the electric fields. If one uses appropriate polarizabilities, the dipole moments are derived from Eq. (2). We adopted the values of 1.15 ($\alpha^{K+}$) and 6.29 ($\alpha^{I-}$) (Å$^3$), which were estimated systematically from experimental refraction data assuming the Clausius-Mossotti relation.[14,15] Thus the dipole moments of the top-layer ions are determined self-consistently. Next, the dipole moments of the second-layer ions were determined in a quite same manner considering the

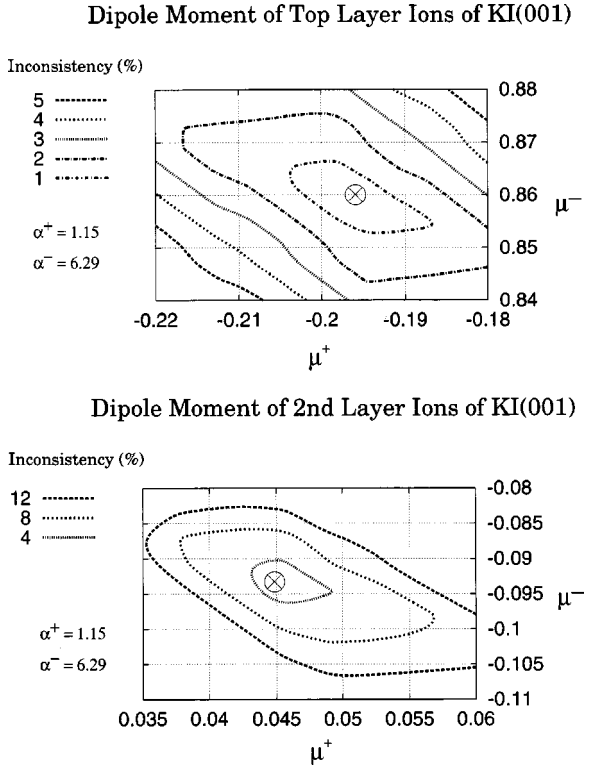


FIG. 4. Contour plots of equi-inconsistency (%) for the dipole moments of the top-layer (a) and second-layer (b) ions. The final self-consistent values are indicated by the symbol ⊗ (see Table II).

dipole moments of the top- and second-layer ions only. Then we calculated again the electric fields at the top-layer ions considering the dipole moments of the second-layer ions determined above.

Figures 4(a) and 4(b) shows the contour plots of equi-inconsistency (%) for $(\vec{\mu}_1^+, \vec{\mu}_1^-)$ and $(\vec{\mu}_2^+, \vec{\mu}_2^-)$, respectively. Such self-consistent and iterative calculations derived the dipole moments of the top- and second-layer ions ($\mu_1^{K+} = -0.196$, $\mu_1^{I-} = 0.86$, $\mu_2^{K+} = 0.044$, $\mu_2^{I-} = -0.094$ in Debye units: $10^{-18}$ esu cm). The result is listed in Table II and compared with the shell model calculation.

Recently, the polarizabilities of alkali-halide crystals were calculated based on first-principles density functional theory.[16] However, the predicted values are considerably different from those derived from experimental optical data coupled with the Clausius-Mossoti relation.[14,15] It is worth to note that polarization of an ion or atom in solids cannot be defined uniquely in a quantum mechanical sense because the wave functions of valence electrons are not localized completely and rather overlap each other at unit-cell boundaries.[17]

TABLE II. Dipole moments (in Debye units: $10^{-18}$ esu cm) of the top- and second-layer $K^+$ and $I^-$ ions determined self-consistently from the MEIS displacement data and those given by shell models (Refs. 5 and 7). In the present calculation, the polarizabilities given by Jaswal and Sharma (Ref. 15) were used. The plus sign means the direction toward the vacuum side.

| | $(\alpha^+)$ | $(\alpha^-)$ | $\mu_1^+$ | $\mu_1^-$ | $\mu_2^+$ | $\mu_2^-$ |
|---|---|---|---|---|---|---|
| Present MEIS | 1.15 | 6.29 | −0.196 | +0.860 | +0.044 | −0.094 |
| Shell model[a] | 1.14 | 5.85 | −0.161 | +1.061 | +0.034 | −0.381 |
| Shell model[b] | 2.28 | 4.51 | −0.218 | +0.456 | +0.024 | −0.078 |

[a]Reference 5.
[b]Reference 7.

TABLE III. Deviations (Å) of the equilibrium positions of the top-layer $K^+$ and $I^-$ planes from those determined by MEIS. The values in the column of RT are time averaged considering thermal vibrations at RT ($\langle u_K \rangle = 0.195$ Å, $\langle u_I \rangle = 0.19$ Å).

| | Benson[a] | | Catlow[b] | | Sangster[c] | | Hellmann[d] | |
|---|---|---|---|---|---|---|---|---|
| | $K^+$ | $I^-$ | $K^+$ | $I^-$ | $K^+$ | $I^-$ | $K^+$ | $I^-$ |
| 0 K | −0.08 | +0.05 | −0.08 | +0.06 | −0.07 | +0.06 | −0.01 | +0.04 |
| RT | −0.05 | −0.02 | −0.04 | +0.04 | −0.04 | +0.04 | +0.04 | +0.03 |

[a]Reference 5.
[b]Reference 11.
[c]Reference 18.
[d]Reference 19.

Now, we consider a balance between the long-range force and the short-range one at the relaxed lattice positions determined above. As the short-range interaction, the Born-Mayer- and Hellmann-type pair potentials were employed.[5,11,18,19] They are written by

Born-Mayer (Refs. 5, 11, and 18):

$$V_S^B(r_{ij}) = A \exp[-r_{ij}/\rho] - C/r_{ij}^6 - D/r_{ij}^{-8}, \tag{3}$$

Hellmann (Ref. 19):

$$V_S^H(r_{ij}) = \frac{A}{r_{ij}} \exp[-r_{ij}/\rho] - C/r_{ij}^6 - D/r_{ij}^8, \tag{4}$$

where the coefficients $A$, $C$, $D$, and $\rho$ take different values for different ion (cation, anion) combinations. The first term corresponds to a repulsive potential, and the second and third ones are the effective van der Waals interactions between two dipoles induced by a fluctuation of electron charge distributions. The long-range Coulombic potentials between two ions $i$ and $j$ were calculated by the modified Ewald method, where only the dipole moments of the top- and second-layer ions determined by MEIS were used and the dipole-dipole interaction was neglected because of its small contribution (three orders of magnitude lower than the point-charge–point-charge interaction). We calculated the total potential energies for the top-layer $K^+$ and $I^-$ ions independently as a function of the displacement of the top-layer $K^+$ or $I^-$ plane from the corresponding relaxed plane determined by MEIS. Here we considered the displacements of the top and second layers only and assumed no relaxation and rumpling for deeper layers. The displacements of the top-layer $K^+$ and $I^-$ planes giving a minimum total potential energy are shown in Table III for some pair potentials.[5,11,18,19] Here the displacement values are time-averaged considering ther-

mal vibrations at RT [in the column (RT)]. All pair potentials give small deviations within 0.05 Å.

### IV. MD SIMULATIONS

The MD simulation program used here is basically similar to the previous one.[2,11] There are two improved points: (1) the potential induced by dipole moments is also calculated by the modified Ewald method and (2) an optimum convergence parameter[13,20] was chosen to minimize the reciprocal lattice sum in the above potential calculations by the Ewald method without lowering the accuracy. In addition, a special attention was paid to make the nearest-neighbor distance in the basic cell equal to equilibrium time-averaged one for each pair potential. The ions vibrate thermally around the lattice site position, which gives a minimum potential energy. If the above matching is insufficient, the interlayer distances in the surface normal direction are significantly shrunk or expanded. Such a situation is seen for the Hellmann-type potential, and a good matching was obtained by changing the parameter $A$, which reflects the ionic radii.

The present MD simulation derives rms thermal vibration amplitudes at RT averaged over all ions in one basic and eight image cells. The basic cell consists of $8\times8$ (lateral plane) $\times 20$ (surface normal direction) ions, which is surrounded by 8 image cells of the same size. The basic cell size is $L\times L\times 5L/2$ ($L=8d_{\mathrm{bulk}}$), and it has fixed boundaries in the lateral plane and free boundaries in the surface normal direction. Lateral oscillation modes with wavelengths larger than $2\times L$ cannot occur in such a limited space. However, their contributions are expected to be small at RT, because primary ones come from the waves with frequency close to $\omega_D$ (Debye frequency). The MD simulations were performed using the pair potentials mentioned before[5,11,18,19] and the dipole moments of the top- and second-layer ions which were determined in the present study. For comparison, the dipole moments given by Benson and Claxton[5] were also employed. The MD simulations for KI(001) and RbI(001) revealed a strong dependence of the pair potential on the bulk TVA's and a small dependence of the dipole moments and pair potential on the enhancement of the top-layer ions. As will be shown later, the combination of the dipole moments determined here and the pair potential proposed by Catlow *et al.*[11] gives a good agreement with the bulk TVA's of $I^-$ and $K^+$ ions derived by the present MEIS analysis.

Figure 5 shows the one-dimensional rms TVA's of the $I^-$ and $K^+$ ions from the top down to the tenth layer of KI(001) calculated from the MD simulation using the dipole moments determined in the present study and the pair potential proposed by Catlow *et al.* The TVA's were also calculated using other pair potentials and those from the top- down to the fifth-layer ions are listed in Table IV. It is clearly seen that the TVA's of the top-layer ions in the surface normal direction are significantly enhanced by 20%–40% compared with those of deeper layer ions. Slightly enhanced are the TVA's of the top-layer ions in the lateral plane and of the second-layer ions in the surface normal direction. According to a simple spring model of solid, the bulk TVA is multiplied by $\sqrt{2}$ to give that of the top-layer atoms in the surface normal direction because the spring constant of the top-layer atoms is reduced to half that for the bulk atoms. In the case of some alloy surfaces, a large enhancements of a factor of 2.5–3 relative to the bulk value was reported[21] recently. Unexpectedly, the enhancement for the top-layer $I^-$ ion with a heavier mass is significantly larger than that of the top-layer $K^+$ ion. It is probably due to the fact that the top-layer $I^-$ ions are displaced toward the vacuum side by 0.1 Å relative to the top-layer $K^+$ ions. Such a situation is quite the same as that for RbI(001) surfaces. The TVA's in the deep region take constant and almost mass-independent values for any pair potentials, although the absolute values strongly depend on the pair potential. The TVA's are intimately related to the slope of the short-range potential for $K^+$-$K^+$ and/or $I^-$-$I^-$ pairs around the position which gives a minimum potential energy. Apparently, a steep slope yields a strong elastic force and thus leads to small vibration amplitudes.

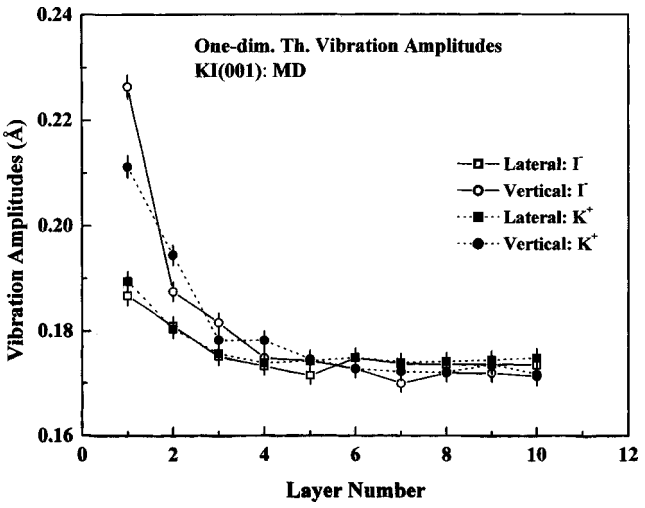


FIG. 5. One-dimensional rms thermal vibration amplitudes for each layer of KI(001) derived from MD simulations. Solid and open symbols denote $K^+$ and $I^-$ ions, respectively, and squares and circles correspond to vibrations in the surface ($x$,$y$) plane and surface normal direction ($z$, [001]), respectively. In the MD simulation, the dipole moments determined in the present analysis and the pair potential proposed by Catlow *et al.* (Ref. 11) are assumed.

If one employs the Debye model assuming a linear dispersion relation coupled with the virial theorem,[22] one obtains the following one-dimensional rms TVA ($\sqrt{\langle u^2\rangle} \equiv \langle u\rangle$) at temperature $T$ (K):

$$\langle u^2\rangle = \frac{1}{3NM}\int_0^{\omega_D}\left\{\frac{1}{\exp(\omega\hbar/k_BT)-1}+\frac{1}{2}\right\}\frac{\hbar Z(\omega)}{\omega}d\omega, \tag{5}$$

where $M$, $N$, $\hbar$, and $k_B$ are ion mass, an atomic density, the Planck constant, and the Boltzmann constant, respectively. In the Debye approximation, the density of states $Z(\omega)$ is equal to $9N/\omega^2\omega_D^3$. Equation (5) indicates that an rms TVA is proportional to $M^{-1/2}$. If this formula is applied to the KI crystal, the TVA's of $K^+$ and $I^-$ at RT are deduced to be 0.258 and 0.143 Å, respectively, using the Debye tempera-

TABLE IV. The rms TVA's (Å) for KI(001) calculated from MD using the dipole moments determined in the present study and the pair potential of (i) Catlow *et al.* (Ref. 11), (ii) Sangster (Ref. 18), and (iii) Hellmann type (Ref. 19). The uncertainty is estimated to be ±0.001 Å.

| | Top layer | | Second layer | | Third layer | | Fourth layer | | Fifth layer | |
|---|---|---|---|---|---|---|---|---|---|---|
| (i) Catlow *et al.* | Vertical | Lateral | Vertical | Lateral | Vertical | Lateral | Vertical | Lateral | Vertical | Lateral |
| $K^+$ | 0.2112 | 0.1894 | 0.1944 | 0.1804 | 0.1782 | 0.1757 | 0.1782 | 0.1739 | 0.1746 | 0.1742 |
| $I^-$ | 0.2263 | 0.1867 | 0.1875 | 0.1809 | 0.1816 | 0.1752 | 0.1749 | 0.1732 | 0.1743 | 0.1715 |
| (ii) Sangster | | | | | | | | | | |
| $K^+$ | 0.1926 | 0.1680 | 0.1701 | 0.1568 | 0.1588 | 0.1556 | 0.1557 | 0.1576 | 0.1539 | 0.1565 |
| $I^-$ | 0.1989 | 0.1594 | 0.1568 | 0.1492 | 0.1507 | 0.1464 | 0.1477 | 0.148 | 0.1477 | 0.1466 |
| (ii) Hellmann type | | | | | | | | | | |
| $K^+$ | 0.1738 | 0.1370 | 0.1556 | 0.1338 | 0.1431 | 0.1304 | 0.1392 | 0.1304 | 0.1342 | 0.1328 |
| $I^-$ | 0.1799 | 0.1364 | 0.1538 | 0.134 | 0.1454 | 0.1310 | 0.1378 | 0.1306 | 0.1362 | 0.1335 |

ture of 130 K for KI.[23] Here we must note that this expression is valid for monatomic materials.

The correlations between the $i$th- and $j$th-layer ($i,j=1,2,...,20$) ions were calculated for the [001], [101], and [111] strings by MD. Now, we define the correlation coefficient between the $i$th-and $j$th-layer ions by the following relation:

$$C_{ij}=\langle u_i\cdot u_j\rangle/\sqrt{\langle u_i\cdot u_i\rangle\cdot\langle u_j\cdot u_j\rangle}, \tag{6}$$

where $u_i$ is the displacement of the ion $i$ from its equilibrium position and the brackets mean a time average. The plus sign indicates the ions moving each other toward the same direction (correlated or positive correlation), whereas the minus sign means the ions moving each other in an opposite side (anticorrelated or negative correlation). The correlations between the top- and $n$th-layer ($n=2,3,...$) ions and between the second- and $n$th-layer ions ($n=1,3,4,...$) in the [001] string for KI(001) are shown, respectively, in Figs. 6(a) and 6(b). There is no significant difference between the $K^+$ and $I^-$ ion termination except for correlations between the top two nearest-neighbor ions in the surface normal direction. Strong correlations are seen between the nearest-neighbor ions, and quite reasonably the larger the distance between the ions, the smaller the correlations. In addition, the $C_{ij}$ value is almost equal to the $C_{i+nj+n}$ value ($n=1,2,...$). The correlations between the top- and $n$th-layer ions in the [101] and [111] strings are shown Figs. 7(a) and 7(b). In the case of the [101] string with the same positive ($+e$) or negative ($-e$) point charges, unexpectedly the correlations between the nearest-neighbor ions are positive (about +0.2), not negative in spite of the same charge lineup of the ions. It indicates that the short-range interaction dominates the lattice motion.

## V. LATTICE DYNAMICS

In order to decompose precisely a MEIS spectrum into the scattering component from each atomic layer, it is essential to obtain knowledge of the energy loss and straggling for the He ions backscattered from near-surface atoms. In a channeling or blocking trajectory, He ions pass in the vicinity of the target nucleus of ion $i$. In this case, the ion suffers an additional energy loss $\Delta E_1(i)$ compared with that $[\Delta E_2(\mathrm{KI})]$ for He ions passing through a medium in a random trajectory far from a target nucleus. We analyzed several MEIS spectra observed under channeling-blocking and random geometries, where the surface peaks were clearly decomposed. In the case of the [101] incidence and the $[10\bar{1}]$ emergence, the energy interval $\Delta E^{12}$(I-I) between the scattering components from the top- and second-layer $I^-$ ions is approximated to be $2\Delta E_1(\mathrm{I})+2\sqrt{2}d_{\mathrm{bulk}}\Delta E_2(\mathrm{KI})$. The corresponding MEIS spectrum is shown in Fig. 8. For He ions incident along the [101] axis and backscattered to 80° in a random direction (see Fig. 2), the energy interval $\Delta E^{12}$(I-I) is approximately $\Delta E_1(\mathrm{I})+(\sqrt{2}+1/\cos 35°)d_{\mathrm{bulk}}\Delta E_2(\mathrm{KI})$. The $\Delta E_1(i)$ and $\Delta E_2$(KI) values for incident energy take slightly different values from those for emerging energy. As a first approximation, we neglected the difference because of a weak energy dependence of the stopping powers. Such a systematic spectrum analysis gives the values of $0.15\pm0.01$ keV/$I^-$, $0.10\pm0.01$ keV/$K^+$, and $0.014\pm0.002$ keV/Å, respectively, as $\Delta E_1$(I), $\Delta E_1$(K), and $\Delta E_2$(KI), for 70-keV $He^+$ incidence. Thus the peak position of the He ions backscattered from each atomic layer is clearly decided. Then the surface peak in an observed MEIS spectrum is decomposed uniquely into the scattering component from each atomic layer assuming a Gaussian shape.

Prior to analyzing the observed MEIS spectra, how to calculate the normalized scattering yields under a single or double-alignment condition is briefly explained. Here the normalized scattering yield for the $n$th-layer ions is defined by the ratio of the total scattering yield from the $n$th-layer ions to that from the top-layer ions. The details of the method are described in the literature.[24,25] First, we define the probability that the lattice site ions from the top down to $n$th layer in the [$hkl$] string ($z$ axis) take the positions $\vec{r}_1(x_1,y_1)$,

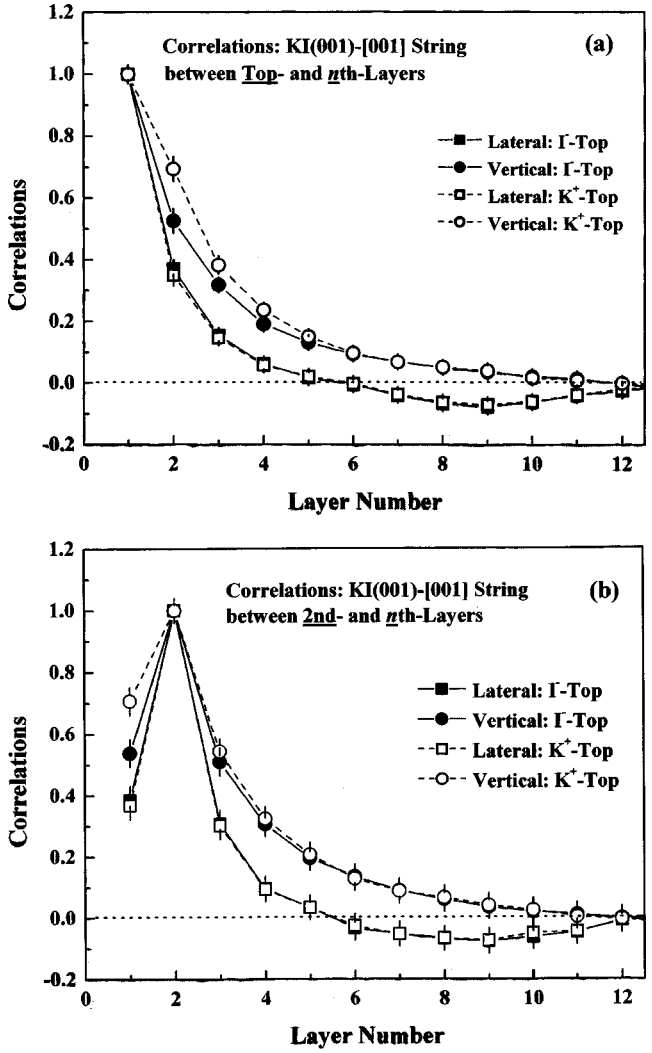


FIG. 6. Correlations between the top- and $n$th-layer ions (a) and between the second- and $n$th-layer ions (b) in the [001] string. Solid and open symbols denote the $I^-$- and $K^+$-terminated [001] string, respectively. Circles and squares indicate the vibrations in the surface normal ([001]) and in the lateral plane ([100] and [010] directions), respectively.

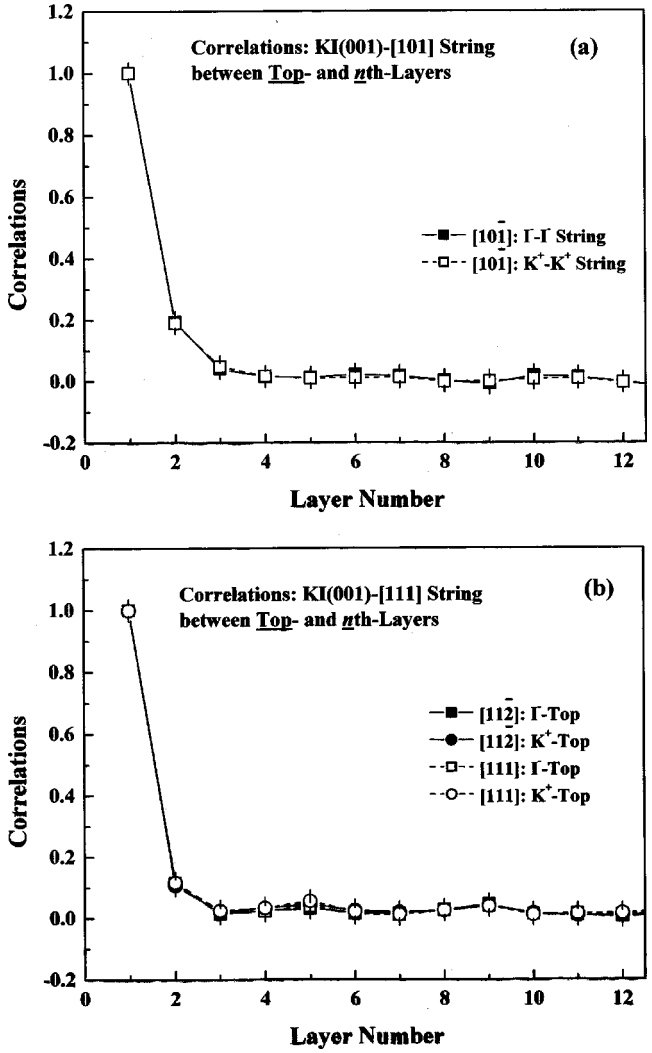


FIG. 7. Correlations between the top- and $n$th-layer ions for the [101] (a) and [111] (b) strings. In the case of the [101] string, solid and open squares denote the $I^-$-$I^-$ chain and the $K^+$-$K^+$ chain, respectively.

$\vec{r}_2(x_2,y_2),\ldots,\ \vec{r}_n(x_n,y_n)$. It is expressed by the following relation:

$$\varphi(\xi_1,\xi_2,\ldots,\xi_{2n}) = \frac{1}{\sqrt{(2\pi)^{2n}|C|}} \times \exp\left\{-\frac{1}{2}\sum_{i=1}^{2n}(C)_{ij}^{-1}\cdot\xi_i\cdot\xi_j\right\}, \quad (7)$$

where $\xi_i \equiv x_i/\langle u_i\rangle$ ($i$ odd) or $\xi_i \equiv y_i/\langle u_i\rangle$ ($i$ even) and $C$ is the correlation matrix $(2n\times 2n)$ defined by Eq. (6). By a Monte Carlo (MC) simulation of ion trajectories we calculate the close encounter probability $P_{CL}(n)$ that the ions are incident along the $[hkl]$ axis and hit the $n$th-layer ion. Of course, all the $P_{CL}(n)$ values are equal to unity if ions are incident along a random direction. It is given by

$$P_{CL}(n) = (S/N_0)\sum_{j=1}^{N}\varphi(\vec{r}_1,\vec{r}_2,\ldots,\vec{r}_{n-1},\vec{r}_0+\vec{\nabla}_n), \quad (8)$$

where $\vec{r}_n = \vec{r}_0 + \vec{\nabla}_n$ ($\vec{r}_0$ is the incident position vector in the first atomic plane), $S$ is the area in which the incident ion positions are confined, and $N_0$ denotes the number of incident ions in the MC simulation. Next, assuming time-reversal symmetry, we calculate the close encounter probability $P'_{CL}(n)$ that the ions are incident along the outgoing path and hit the $n$th-layer ion.[24,25] This assumption is adequate if the scattering point is shallow enough and thus the energy loss is negligibly small. The normalized scattering yield for the $n$th-layer ion under a double alignment condition is given by

$$Y(n) = P_{CL}(n)\times P'_{CL}(n). \quad (9)$$

In this approximation, the incident and exit paths are treated independently.

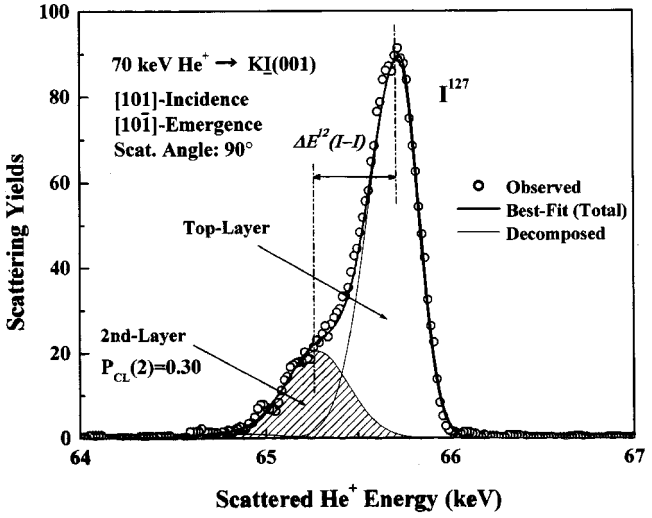


FIG. 8. Observed (open circles) and best-fitted (solid curves) MEIS spectra for 70-keV $He^+$ ions incident along the [101] axis and backscattered from $I^-$ ions to the $[10\bar{1}]$ direction. The energy interval between the deconvoluted first- and second-surface peaks $\Delta E^{12}$ I-I is estimated to be 0.45 keV.

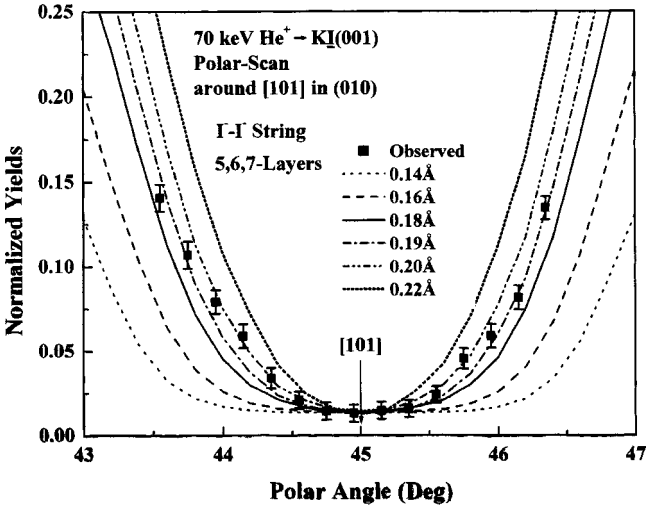


FIG. 9. Observed (squares) and simulated (curves) polar-scan spectra for the scattering components from the fifth- to seventh-layer $I^-$ ions. Here 70-keV $He^+$ ions were incident around the [101] axis and backscattered to 80° in the (010) plane.

We first determine directly the rms TVA's of the bulk $K^+$ and $I^-$ ions by a polar-scan analysis of MEIS. As mentioned before, Fig. 2 indicates the observed and best-fitted MEIS spectra for 70-keV $He^+$ incident along the [101] axis of KI(001) and backscattered from $I^-$ to 80°. We put an energy window for the scattering components from the fifth- to seventh-layer $I^-$ ions (64.7–65.5 keV) and performed the polar scan around the [101] axis in the (010) plane. It was found that such a polar-scan spectrum around the angle giving a scattering yield minimum for the scattering components from deep layers was not sensitive to correlations and enhancement of thermal vibrations but dependent significantly on the rms TVA's of the lattice site ions in depth. Figure 9 shows the observed polar-scan spectrum together with the simulated ones assuming the vibration amplitudes of $I^-$ ions to be 0.14, 0.16, 0.18, 0.19, 0.20, and 0.22 Å. The $\langle u_I \rangle$ value of $0.19 \pm 0.01$ Å gives the best fit to the observed spectrum. A similar polar scan was also performed for the scattering components from the fifth- to the eighth-layer of $I^-$ ions around the [111] axis in the $(11\bar{1})$ plane. It must be noted that the $K^-$ and $I^-$ ions are alternately lined up in the [111] string. We tried to best-fit the simulated spectrum to the observed one by varying the $\langle u_K \rangle$ value. However, the fitting parameter $\langle u_K \rangle$ giving a best fit widely ranges from 0.14 to 0.24 Å because the $I^-$ ions dominate the [111] string potential.

We simplify the lattice motion and consider $\langle u_I \rangle$, $\langle u_K \rangle$, the correlations between neighboring ions, and the vertical enhancement of the top-layer ions only the correlations between the ions in the [111] string, were neglected because of their small values less than 10% from the MD simulations. The above approximation seems reasonable from the MD simulations presented before (Figs. 6 and 7). Here we define the enhancement factor $\beta_i$ as $\langle u_{K\perp}(1) \rangle = \beta_K \langle u_K \rangle$ and $\langle u_{I\perp}(1) \rangle = \beta_I \langle u_I \rangle$ for the top-layer $K^+$ and $I^-$ ions, respectively, in the surface normal direction. In order to determine these values, the MEIS measurements were performed under five different scattering conditions (see Fig. 10). The close encounter probability for the second-layer $I^-$ ions ($P_{CL}^{101}$(2,I-I)) is derived to be 0.55 by decomposing the MEIS spectrum observed for the [101] incidence and random emergence (see Fig. 2). The normalized scattering yield for the second-layer $I^-$ ions is determined to be 0.30 from the MEIS spectrum observed under the double-alignment geometry of the [101] incidence and $[10\bar{1}]$ emergence (see Fig. 8). These results are quite consistent from the view point of time-reversal symmetry[24] presented before ($0.55 \times 0.55 \approx 0.30$). Now, we consider the scattering geometry indicated in Fig. 10(b). The probability to hit the second-layer $I^-$ ions [$P_{CL}^{101}(2,\text{I-I}) = 0.55$] is already known. The normalized scattering yield is derived to be 0.40 from the MEIS spectrum

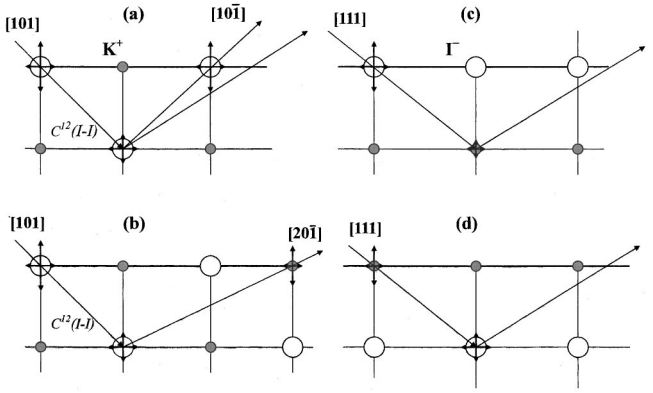


FIG. 10. Side views of various scattering geometries: (a) [101] incidence and $[10\bar{1}]$ and random emergence, (b) [101] incidence and $[20\bar{1}]$ emergence, (c) [111] incidence and random emergence (scattered to 60° from the second-layer $K^+$ ions), (d) [111] incidence and random emergence (scattered to 60° from the second-layer $I^-$ ions).

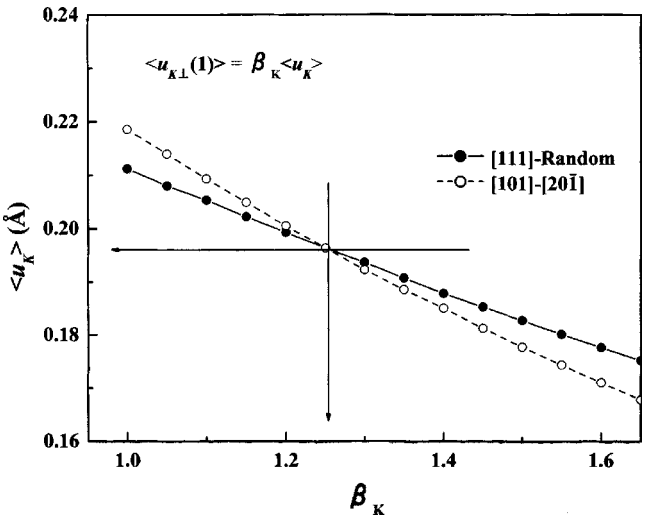


FIG. 11. Points ($\beta_K\langle u_K\rangle$) satisfying the $P_{CL}^{111}$ (2, K-I) and $P_{CL}^{201}$ (2, I-I) values derived from the MEIS analysis are plotted as solid and dashed curves, respectively. The crossing point gives the $\beta_K$ and $\langle u_K\rangle$ values.

observed under this condition ([101] incidence and $[10\bar{1}]$ emergence). This normalized scattering yield is equated to $P_{CL}^{101}(2,\text{I-I})\times P_{CL}^{201}(2,\text{I-I})$ from the time-reversal symmetry. In fact, the energy of He ions scattered to the $[20\bar{1}]$ direction is 67.0 keV, which is almost equal to the incident energy (70 keV). If the $\langle u_K\rangle$ and $\beta_K\langle u_K\rangle$ values ($\langle u_I\rangle$ is already known) are given, one can calculate the $P_{CL}^{201}(2,\text{K-I})$ by the MC simulation of ion trajectories. Next, we look at the scattering geometry indicated in Fig. 10(d). Also, in this case, the normalized scattering yield [$=P_{CL}^{111}(2,\text{K-I})$] is calculated from MC simulations assuming the $\langle u_K\rangle$ and $\beta_K\langle u_K\rangle$ values. We measured the MEIS spectrum for the [111] incidence and random emergence (scattering angle 60°) and obtained a normalized scattering yield of 0.78. Figure 11 shows the combinations ($\langle u_K\rangle,\beta_K$) which give the above $P_{CL}^{201}(2,\text{I-I})$ and $P_{CL}^{111}(2,\text{K-I})$ values. Thus we obtain the $\langle u_K\rangle$ and $\beta_K$ values as the cross point of the two curves ($\langle u_K\rangle = 0.196\pm 0.015$ Å and $\beta_K = 1.26\pm 0.10$). If $\langle u_K\rangle$ is known, we can determine the $\beta_I\langle u_I\rangle$ value from the MEIS measurement under the scattering geometry indicated in Fig. 10(c) and have obtained the enhancement factor ($\beta_I$) of $1.10\pm 0.10$.

Finally, the correlations between the top- and second-layer ions in the [101] and [001] strings are determined in quite the same manner as mentioned above. As can be seen from Fig. 10(a), the correlation coefficient $C_{12}$(I-I) for the [101] string in its perpendicular direction ($[10\bar{1}]$) is determined to be $0.05\pm 0.05$ from the MEIS spectrum analysis [$P_{CL}^{101}(2,\text{I-I})=0.55$] followed by MC simulation of ion trajectories. In this case, the scattering component from the third-layer $I^-$ ions contributes significantly to the surface peak. However, the correlation between the top- and second-layer $I^-$ ions is almost the same as that between the second- and third-layer $I^-$ ions. In addition, the correlations between the second-nearest-neighbor ions are negligibly small. We considered the above situations when decomposed the surface peak. The correlation coefficient $C_{12}$(K-I) for the [001] string in the lateral direction ([100] and [010]) can be also determined in quite the same manner. The MEIS measurements were performed under the conditions that 70-keV $He^+$ ions were incident along the [001] incidence and backscattered to the $[60\bar{1}]$ direction and to the direction 1.8° off from the $[60\bar{1}]$ in the (010) plane. As expected, we obtain the strong correlation of the $C_{12}$(K-I) value of $0.40\pm 0.05$ in the vertical direction of the [001] string.

TABLE V. The bulk TVA's ($\langle u_I\rangle$, $\langle u_K\rangle$), enhancement coefficients ($\beta_I$, $\beta_K$) for top-layer ions, and correlation coefficients [$C_{12}$(I-I)$=C_{23}$(I-I)] for the [001] and [101] strings.

(i) Thermal vibration amplitudes (bulk)

| | $\langle u_I\rangle$ (Å) | $\langle u_K\rangle$ (Å) |
|---|---|---|
| $\Theta_D = 130$ K[a] | 0.143 | 0.258 |
| Shell model[b] | 0.180 | 0.185 |
| MD (Catlow[c]) | $0.175\pm 0.005$ | $0.175\pm 0.005$ |
| MD (Sangster[d]) | $0.145\pm 0.008$ | $0.155\pm 0.008$ |
| MD (Hellmann[e]) | $0.130\pm 0.005$ | $0.130\pm 0.005$ |
| Present MEIS | $0.190\pm 0.010$ | $0.196\pm 0.015$ |

(ii) Enhancement coefficients for the top-layer ions in the surface normal direction

| | $\beta_I$ | $\beta_K$ |
|---|---|---|
| MD (Catlow) | $1.29\pm 0.05$ | $1.20\pm 0.05$ |
| MD (Sangster) | $1.37\pm 0.07$ | $1.25\pm 0.07$ |
| MD (Hellmann) | $1.38\pm 0.05$ | $1.34\pm 0.05$ |
| Present MEIS | $1.10\pm 0.10$ | $1.26\pm 0.10$ |

(iii) Correlation coefficients between the nearest-neighboring $I^-$-$I^-$ ions in the perpendicular directions of the [001]-($I^-$-$K^+$) and [010]-($I^-$-$I^-$) strings.

| | $C_{12}^{001}$(I-K) | $C_{12}^{101}$(I-I) |
|---|---|---|
| MD (Catlow) | $0.35\pm 0.02$ | $0.15\pm 0.02$ |
| MD (Sangster) | $0.25\pm 0.05$ | $0.15\pm 0.05$ |
| MD (Hellmann) | $0.28\pm 0.02$ | $0.15\pm 0.$ |
| Present MEIS | $0.40\pm 0.05$ | $0.05\pm 0.05$ |

[a]Reference 23.
[b]Reference 26.
[c]Reference 11.
[d]Reference 18.
[e]Reference 19.

The results obtained are shown in Table V and compared with the predictions of the shell model[26] and the MD simulations using different pair potentials. Concerning the bulk TVA's, the shell model[26] and MD simulation using the Catlow-type pair potential[11] give consistent values with the present result. On the other hand, the MD simulations using Sangster's and Hellmann's potentials result in considerably smaller values. In any cases, the bulk TVA's are almost mass independent, in contrast to those calculated from the Debye approximation. Small enhancements were found for the top-layer $K^+$ and $I^-$ ions in the surface normal direction. Concerning the correlations, those observed are large for the [001] string in the lateral direction, but small for the [101] string in the $[10\bar{1}]$ direction, as expected. Overall agreement

is obtained between the present results and the MD simulations using the dipole moments determined in the present study and the Catlow-type pair potential.

## VI. CONCLUSION

We determined directly the relaxation and rumpling of the KI(001) surface by high-resolution MEIS. From the displacements of the top- and second-layer ions from the equilibrium lattice positions, their dipole moments were derived self-consistently using the polarizabilitires of $K^+$ and $I^-$ ions estimated from the optical refraction data. Knowledge of the dipole moments makes it possible to test the applicability of the short-range pair potentials proposed so far, which reproduce the elastic constants of the KI crystal. All pair potentials given by Catlow *et al.*,[11] Sangster,[18] and Sipani and Gupta[19] reproduced the relaxed lattice positions determined by MEIS within 0.04 Å.

We also determined directly the bulk TVA's of $K^+$ and $I^-$ ions, the enhancements of the TVA's of the top-layer ions in the surface normal direction, and the correlations between the nearest-neighbor ions in the [101] and [001] strings. The MEIS measurements under various kinds of scattering geometries combined with the MC simulations of ion trajectories made it possible to derive the above values. Concerning the bulk TVA's, the shell model[19] calculation and the MD simulation using the Catlow-type pair potential[11] are consistent with the present result. On the other hand, the MD simulations using the Sangster's and Hellmann's potentials give considerably smaller values. In any cases, the bulk TVA's are almost mass independent, in contrast to those calculated from the Debye approximation. Small enhancements were found for the top-layer $K^+$ and $I^-$ ions in the surface normal direction. Such considerably small enhancements compared with those observed at metal surfaces are responsible for the stronger bonding of ionic crystals rather than metallic bonds. As expected, we observed a strong correlation in the lateral direction of the [001] string, but a small one in the $[10\overline{1}]$ direction of the [101] string. Overall agreement was obtained between the present results and the MD simulations using the dipole moments determined here and the Catlow-type pair potential.

## ACKNOWLEDGMENTS

The authors would like to appreciate Y. Hoshino and Y. Yagi for their assistance in carrying out the MEIS experiments and the MC simulation analysis.

*Corresponding author. FAX: +81-77-561-2710/2657. Electronic address: ykido@se.ritsumei.ac.jp

[1] J. P. LaFemina, in *Handbook of Surface Science*, edited by W. N. Unertl (Elsevier, Amsterdam, 1996), Vol. 1, Chap. 4.
[2] T. Nishimura, A. Ikeda, H. Namba, and Y. Kido, Surf. Sci. **411**, L834 (1998).
[3] T. Okazawa, Y. Hoshino, T. Nishimura, and Y. Kido, J. Phys.: Condens. Matter **13**, 9835 (2001).
[4] J. Vogt and H. Weiss, Surf. Sci. **491**, 155 (2001).
[5] G. C. Benson and T. A. Claxton, J. Chem. Phys. **48**, 1395 (1968).
[6] M. R. Welton-Cook and M. Prutton, Surf. Sci. **64**, 633 (1977).
[7] F. W. de Wette, W. Kress, and U. Schröder, Phys. Rev. B **32**, 4143 (1985).
[8] W. Kress, F. W. de Wette, A. D. Kulkarni, and U. Schröder, Phys. Rev. B **35**, 5783 (1987).
[9] K. Kobayashi (private communication).
[10] T. Nishimura, A. Ikeda, and Y. Kido, Rev. Sci. Instrum. **69**, 1671 (1998).
[11] C. R. A. Catlow, K. M. Diller, and M. J. Norgett, J. Phys. C **10**, 1395 (1977).
[12] T. Okazawa, S. Ohno, Y. Hoshino, T. Nishimura, and Y. Kido, Nucl. Instrum. Methods Phys. Res. B **183**, 108 (2001).
[13] D. E. Parry, Surf. Sci. **49**, 433 (1975).
[14] J. R. Tessman, A. H. Kahn, and W. Shockley, Phys. Rev. **92**, 890 (1953).
[15] S. S. Jaswal and T. P. Sharma, J. Phys. Chem. Solids **34**, 509 (1973).
[16] S. Petersson and K. R. Subbaswamy, Phys. Rev. B **42**, 5883 (1990).
[17] D. Vanderbilt and R. D. King-Smith, Phys. Rev. B **48**, 4442 (1993).
[18] M. J. L. Sangster, J. Phys. Chem. Solids **34**, 355 (1973).
[19] S. K. Sipani and V. P. Gupta, Phys. Rev. B **43**, 9924 (1991).
[20] W. Simon, De Leeuw, and J. W. Perram, Mol. Phys. **37**, 1313 (1979).
[21] C. J. Baddeley, L. H. Bloxham, S. C. Laroze, R. Raval, T. C. Q. Noakes, and P. Bailey, J. Phys. Chem. B **105**, 2766 (2001).
[22] G. Marc and W. G. McMillan, Adv. Chem. Phys. **58**, 209 (1985).
[23] J. T. Lewis, A. Lahoczky, and C. V. Briscoe, Phys. Rev. **161**, 877 (1967).
[24] J. F. van der Veen, R. G. Smeenk, R. M. Tromp, and F. W. Saris, Surf. Sci. **79**, 219 (1979).
[25] R. M. Tromp and J. F. van der Veen, Surf. Sci. **133**, 159 (1983).
[26] R. K. Gupta, Phys. Rev. B **12**, 4452 (1975).